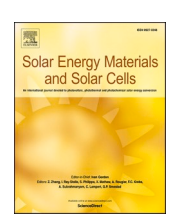
ELSEVIER

Contents lists available at ScienceDirect

Solar Energy Materials and Solar Cells

journal homepage: www.elsevier.com/locate/solmat





Boosting thermochemical performance of SrBr₂·6H₂O with a secondary salt hydrate

Natalia Mazur^{a,b}, Isidoros Kotinis^a, Henk Huinink^{a,b,*}, Hartmut Fischer^c, Olaf Adan^{a,b,c}

- a Department of Applied Physics, Eindhoven University of Technology, Den Dolech 2, 5600, MB Eindhoven, the Netherlands
- ^b Eindhoven Institute for Renewable Energy Systems, Eindhoven University of Technology, PO Box 513, 5600, MB Eindhoven, the Netherlands
- ^c TNO Materials Solutions, High Tech Campus 25, 5656 AE, Eindhoven, the Netherlands

ARTICLE INFO

Keywords: Thermochemical heat storage Salt hydrates Strontium bromide Composite Deliquescence Reaction kinetics

ABSTRACT

This work systematically investigates the effect of 9 inorganic salt hydrates on the performance of strontium bromide (SrBr₂) a thermochemical material (TCM). The goal is to boost the performance of this base salt by enhancing the reaction kinetics of the SrBr₂ 6-1 transition or by shrinking the reaction hysteresis. The study shows that the added salts that do not share a common ion with SrBr₂ (LiCl, LiF, ZnF₂, ZnI₂, K₂CO₃) give limited to no benefits. The lack of improvement is due to a side reaction between SrBr₂ and the added salt leading to the formation of new salt hydrate with low hygroscopicity that does not contribute to the thermochemical reaction. The addition of hygroscopic bromide salts with divalent cations (ZnBr₂, CaBr₂, MnBr₂) gave mixed results depending on the sample history. The most likely cause is cation exchange between bromide salts occurring during exposure to high vapour pressures which promote ionic mobility. The overall best performance was achieved with the addition of LiBr, which we attribute to its high hygroscopicity.

1. Introduction

Despite our efforts in the ongoing energy transition, only 7% of current energy in Europe is generated from fully renewable sources, such as wind, solar or hydro [1]. Nonetheless, to achieve the desired changes in our environment, this share must be tripled at the very least [2], or the utilisation of other energy sources, such as waste heat, must be increased. Unfortunately, one of the main challenges connected to the greater utilisation of renewable energy sources stems from their inherent temporal and spatial mismatch. To solve this issue and bridge the gap between energy generation and consumption, energy storage is needed. Since energy comes in many forms, various solutions are needed. One such solution is heat storage, since a large proportion of energy, especially in households, goes towards space and water heating [3]. Once again, we are presented with several possibilities [4], where thermochemical heat storage (TCHS) in salt hydrates is one of them [5-7]. Over the past years, dozens of salt hydrates were tested for their suitability as thermochemical materials (TCMs), and the reaction of strontium bromide hexahydrate (SrBr₂·6H₂O, Reaction 1) has been frequently brought forward as a promising candidate [8-10].

$$SrBr_2 \bullet H_2O(s) + 5H_2O(g) \leftrightarrow SrBr_2 \bullet 6H_2O(s) + Heat$$
 (Rx.1)

There are two primary reasons why $SrBr_2 \cdot 6H_2O$ is considered to be a promising TCM. Firstly, the hydration reaction can provide enough heat to cover the residential needs, while the opposite dehydration reaction, which recharges the system, is achievable well below $100\,^{\circ}C$, when exposed to atmospheric humitidy conditions [8], a temperature easily generated by for example, commercial solar thermal collectors. Secondly, $SrBr_2 \cdot 6-1$ transition has a high theoretical energy density of 945 kJ/kg (1.99 GJ/m³) $SrBr_2 \cdot 6H_2O$ and an effective energy density of 798 kJ/kg [10].

SrBr $_2$ 6-1 reaction has been extensively studied in the literature on the lab scale and in prototypes [8,11]. The challenges related to using SrBr $_2$ as TCM that are being tackled by other reserchers are agglomeration and low thermal conductivity when used in its pure form. Botch issues are often tackled by developing a composite material. Most commonly an (inert) matrix it employed, such as vermiculite [8,12,13], silica gel [14], metal organic frameworks [15] or silicone foam [16] to prevent the agglomeration. To enhance thermal conductivity, expanded graphite [17–19], also in combination with polymeric binders [20–22], was used. Although the use of a matrix usually resulted in greater mechanical stability and thermal conductivity than the pure salt and sometimes even enhanced reaction kinetics due to the particles' greater permeability, it was done at the expense of energy density.

^{*} Corresponding author. Department of Applied Physics, Eindhoven University of Technology, Den Dolech 2, 5600, MB Eindhoven, the Netherlands. E-mail address: h.p.huinink@tue.nl (H. Huinink).

Table 1 Secondary salt matrix compiling DRH values [%RH] at 20–25 °C [42, 43]. The cells are coloured according to the following criteria: Green: $p_{del} \leq p_{eq}$ Yellow: $p_{del} \leq p_{hyd}$, Orange: $p_{del} < p_{del}$ srBr2 Grey: $p_{del} > p_{del}$ srBr2. Dark shades indicate materials that are tested, while light shades are potential candidates that fulfil the criteria but are not tested. SrBr2 is highlighted in blue.

	F-	Cl ⁻	Br ⁻	ŀ	CO ₃ ²⁻
Li ⁺		11	6.7	18	
Na⁺	96.9	75.3	57.7	38	88
K⁺	30.5	84.3	80.7	68.7	44
Rb⁺	14.5	75	78.5	76.1	
Cs⁺	3.7	65.8	83	90.8	
Mg ²⁺ Ca ²⁺ Sr ²⁺		33	31.5	28	
Ca ²⁺		28.8	16.5	15	
Sr ²⁺		70.8	59	34	
Mn ²⁺		56	34.6		
Zn ²⁺		3	7.7	19	

Nevertheless, the hysteresis between hydration and dehydration, which has been observed in several instances [22,23] has never been resolved. Although this phenomenon is quite common in salt hydrate (de)hydration reactions [24–26], it is undesirable in TCHS applications, as it introduces a range of conditions at which the material does not undergo the desired phase transition. Unfortunately, this phenomenon is often accepted as an inherent material property and only in few investigations studied in a systematic and deliberate manner [27,28].

Studies on the other salt hydrates considered for TCHS have shown that mixing two salt hydrates can achieve enhanced energy density and narrower reaction hysteresis. A greater energy density has been observed in salt mixtures of MgSO₄-MgCl₂, MgSO₄-LiCl, and CaCl₂-KCl [29–33]. Furthermore, a similar approach can lead to enhanced reaction kinetics as in the case of CaCl₂-MgCl₂, MgSO₄-CaCl₂ and K_2CO_3 -Cs₂CO₃ [34–36]. Finally, shrinkage of the hysteresis between dehydration and hydration reaction which has been observed in several instances in salt mixtures of K_2CO_3 and a hygroscopic additive [27,36,37]. Some of the approaches used the deliquescence transition of the added salt. Deliquescence is caused by absorption of excessive amounts of water leading to salt dissolution. Moreover, mixing of two deliquescent compounds will lower their respective deliquescence humidities (DRH). It could be also used to enhance the energy density of the system [38].

Mixing of $SrBr_2$ with another salt hydrate for TCHS applications has been investigated only in the single case to decrease the overall material cost without sacrificing heat storage density or material stability [39]. Additionally, it has been investigated as a phase change heat storage material [40,41] to modify the melting and crystallisation properties of $SrBr_2 \cdot 6H_2O$.

The aim of this work is to investigate the impact of secondary salt

Table 2Results of IC measurements summarising the average composition based on 3 samples and the corresponding standard deviation.

-	
Sample	Composition [mol SrBr ₂ : mol additive]
Sr-LiF	55.7 ± 4.77
Sr-ZnF ₂	35.0 ± 0.28
Sr-LiCl	34.0 ± 1.84
Sr-LiBr	33.7 ± 1.66
Sr-CaBr ₂	42.4 ± 0.20
Sr-MnBr ₂	34.5 ± 5.29
Sr-ZnBr ₂	35.7 ± 1.20
Sr-ZnI ₂	29.9 ± 1.50
Sr-K ₂ CO ₃	28.8 ± 3.72

hydrates on SrBr $_2$ 6-1 transition when used as a low-temperature TCM. The purpose of te secondary salt is to shrink the reaction hysteresis and to improve reaction kinetics close to equilibrium conditions, thus increasing the potential operating window of SrBr $_2$. To select a suitable secondary salt hydrate, we will employ an approach previously developed on K_2CO_3 [37]. The (de)hydration behaviour, cyclic stability, and energy density of the salt mixtures are tested to find the most optimal salt hydrate combination.

2. Materials

2.1. Secondary salt selection procedure

A suitable secondary salt hydrate should fulfil at least one of the following criteria and do not curb any other in a significant way:

- Shrink reaction hysteresis by increasing hydration temperature and/ or decreasing dehydration temperature.
- 2. Increase (de)hydration reaction kinetics.
- 3. Increase energy density.
- 4. Be cyclically stable, i.e. undergo many (de)hydration reactions without degradation of performance or energy density.

The selection procedure for the secondary salt is based on work done on $K_2 CO_3 \bullet 1.5 H_2 O$ [37]. In instance in Table 1, we have compiled deliquescence relative humidity (DRH) values for the most common salt hydrates. The DRH values define conditions at which salt hydrate absorbs so much water that it forms a salt solution, i.e. deliquescence. It is also a measure of salts' affinity for water, as salts with low DRH values undergo deliquescence at relatively dry conditions and thus are highly hygroscopic and highly soluble as well. Consequently, those values were evaluated with respect to deliquescence, equilibrium and hydration vapour pressures of pure $SrBr_2 \bullet 6H_2O$ at $25~C~(p_{del,25C}=31.58~mbar~p_{eq,25C}=2.23~mbar~, p_{hyd,25C}=3.68~mbar~)~[22].$

We expect salts with $p_{del} < p_{eq,~SrBr2}$ will be most effective. However, based on the work done on K_2CO_3 [37], salts with $p_{del} \ll p_{del,~SrBr2} > p_{eq,~SrBr2}$ can be beneficial as well. Based on that, we have selected 9 reference compounds to be tested (dark cells in Table 1). Both ZnF_2 and LiF have been added to the screening as they have very high deliquescent points and thus should not impact (de)hydration behaviour of $SrBr_2$ if hygroscopicity of the secondary salt is the only factor that is of importance.

2.2. Salt mixture preparation

Salt mixtures were prepared through planetary ball milling of $SrBr_2 \bullet H_2O$ with an anhydrous additive. $SrBr_2 \bullet 6H_2O$ purchased from Alfa Aesar was dehydrated to monohydrate in an oven at 60 °C. The additive salts were dehydrated in an oven at 160 °C. In the case of salt hydrates with a low melting point, such as $CaBr_2 \cdot 6H_2O$, the dehydration would be conducted in several steps to prevent the salt's melting.

After dehydration, $SrBr_2 \bullet H_2O$ was roughly ground, and approximately 5 g of the dry powder was transferred to an agate milling jar. Next, an appropriate amount of the secondary salt was added, resulting in a 35:1 mol ratio of anhydrous base salt to an anhydrous additive. The composition was defined based on earlier research conducted on comparable systems [27,28]. The goal is to boost the performance of the base salt, without excessively lowering its deliquescence point.

Finally, ten 10 mm agate milling balls were added to the jar. The salts were milled at 175 rpm for 30 min. After milling, samples were transferred to an airtight glass container for storage.

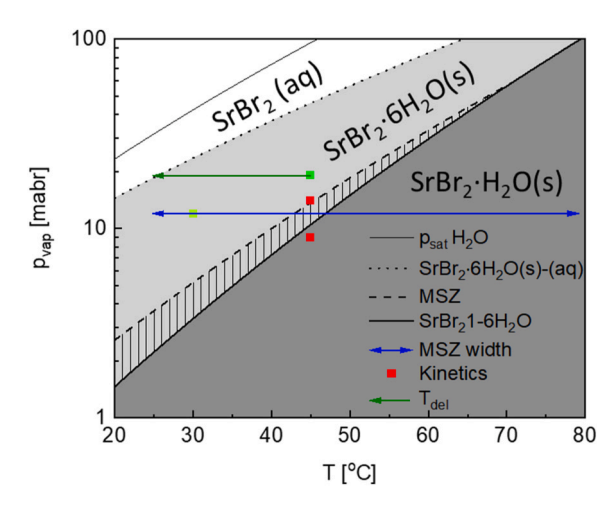


Fig. 1. Phase diagram (water vapour pressure vs temperature) of SrBr₂ adapted from Ref. [22] with stability regions of investigated SrBr₂ hydrates highlighted in grey. The hatched area shows the metastable zone (MSZ), where hydration does not occur instantaneously. The blue arrow shows the temperature scan conducted to determine reaction onset points, while the green arrow shows the temperature scan determining the deliquescence temperature. The red points indicate conditions at which (de)hydration kinetics were measured, while the green squares show conditions at which the sample was hydrated during cycling.

3. Methods

3.1. Sample composition

The composition of the freshly prepared samples was checked with ion chromatography (IC). Three samples of the dry powder, approximately 1 mg each, were dissolved in 10 mL of deionised water. The concentrations of cations and anions were measured with a Dionex ICS-90 ion chromatograph and compared with Dionex standards. Additional standards were prepared from SrBr $_2$ (Alfa Aesar) and NaI (VWR) to measure Sr $^{2+}$ and I $^-$ ion concentration as they are not included in the Dionex standards. The sample composition is determined by comparing the measured molar concentration of Sr $^{2+}$ ions with the molar concentration of either the cation or anion of the additive. The average measured ratios and the standard deviations are presented in Table 2. The secondary salt hydrate in the salt mixture is denoted in the sample name.

The strongest deviation from the intended weighted out ratio is present in Sr-LiF sample. LiF is almost insoluble therefore we believe that the deviation stems from the fact that we did not allow enough time for the entire sample to dissolve. The spread in the remaining compositions most likely stems in the difficulty in handling the highly hygroscopic salts and in obtaining full dehydration without melting or decomposition. Based on earlier work [27] such small variations in the secondary salt content should not affect the behaviour in the base salt in a significant way, as much larger differences in the additive content are needed to impact the based salt in a measurable way.

3.2. Thermogravimetric analysis

Thermogravimetric analysis (TGA) was done in TGA851e by Mettler-Toledo. The device's temperature was calibrated using benzophenone, In, and Zn calibration standards by determining their melting onset point from the heat flow signal. An external humidifier is coupled to the TGA to control humidity inside the TGA oven. The humidifier was calibrated by determining the deliquescence points at 25 °C of LiCl·H₂O, MgCl₂·6H₂O, K₂CO₃·1.5H₂O and Mg(NO₃)₂·6H₂O [42].

Prior to a TGA measurement, sample is sieved between 50 and 164 μm particle fraction. Approximately 5 mg of the sieved powder is loaded

Table 3 Summary of reaction conditions and driving force p_d (p/ p_{eq}) applied during cycling and kinetic investigation.

	Hydration		Dehydration		
	Reaction conditions	Pd	Reaction conditions	p _d	
Screening	45 °C 14 mbar	1.3	45 °C 9 mbar	0.86	
Low p _d cycling High p _d cycling	45 °C 19 mbar 30 °C 12 mbar	1.8 3.6	45 °C 0 mbar 80 °C 0 mbar		

into a 40 μL aluminium pan by Mettler-Toledo, giving a uniform coverage of the bottom of the pan. All experiments were conducted under a nitrogen atmosphere with a fixed flow rate of 300 mL/h.

The measurement procedure was adapted from the earlier study on $K_2CO_3\ [37]$ and the measurement conditions are indicated in Fig. 1 and summarised in Table 3 Summary of reaction conditions and driving force $p_d\ (p/p_{eq})$ applied during cycling and kinetic investigation Table 3. The thermogravimetric measurements can be divided into five categories, which investigate:

- 1) Reaction onset points: A temperature sweep between $80\,^{\circ}$ C and $25\,^{\circ}$ C at a 1 K/min scanning rate was conducted at a fixed vapour pressure of 12 mbar. Between the temperature ramps, a 1 h dwell at $80\,^{\circ}$ C and a 2 h dwell at $25\,^{\circ}$ C were introduced to ensure complete conversion prior to the following heating/cooling step. Onset points for the reaction were determined by looking for a knee point in the 1st derivative of the mass-time curve and the corresponding sample temperature.
- 2) Reaction kinetics: After establishing the reaction onset points, the reaction kinetics were measured at isobaric and isothermal conditions. First, sample was dehydrated in-situ at 80 °C and 0 mbar. After 60 min, the temperature was lowered to 40 °C and equilibrated for 30 min while maintaining dry gas flow. After equilibration, water vapour with a partial pressure of 14 mbar was supplied to the TGA oven, marking the starting time for hydration. The 14 mbar vapour pressure was held constant for 2 h before it was increased to 19 mbar to finalise hydration within 1 h. Subsequently, vapour pressure was lowered to 9 mbar, thus initiating dehydration. Conditions at low driving force, p_d , it is close to equilibrium have been chosen on purpose at reaction kinetics are commonly most inhibited in this area [22].
- 3) Deliquescence temperature and DRH: The sample was fully hydrated at 50 °C and 19 mbar. After that, the temperature was gradually lowered to 25 °C at 1K/min. The deliquescence temperature is taken as the intersection of two tangents drawn at the end of hydration, where stable loading is measured and at the end of the temperature scan, where a rapid mass uptake is recorded.
- 4) Cyclic stability: The selected salt mixtures were subjected to 10 consecutive (de)hydration cycles. First, the sample was dehydrated at 80 °C in dry N_2 flow for 1 h. Afterwards, the temperature was lowered to 45 °C, where it was equilibrated for 30 min in dry N_2 flow. The hydration was conducted at 19 mbar for 90 min. Subsequent dehydration was done at 0 mbar for 60 min. The temperature was fixed at 45 °C for the duration of the cycling measurement. This type of cycling will be referred to as low p_d cycling.
- 5) Impact of cycling on reaction kinetics: The reaction kinetics at isobaric-isothermal conditions described in point 2 were reevaluated on cycled samples. Two sets of cycled samples were prepared. The first set was cycled under conditions described in point 4. The second set was cycled under a wider temperature range. In this material conditioning the dehydration was conducted at 80 °C and 0 mbar. Hydration was conducted at isobaric and isothermal conditions of 30 °C and 12 mbar. A 30 min temperature stabilisation period in dry N₂ at 30 °C is introduced between dehydration and hydration to ensure isobaric-isothermal conditions during hydration.

Table 4 Measured hydration (T_{hyd}) and dehydration (T_{deh}) onset points at 12 mbar water vapour pressure. Calculated MSZ width $(T_{deh} \cdot T_{hyd})$. Measured deliquescence temperature (T_{d}) at 19 mbar water vapour pressure.

Sample	T _{hyd} [°C]	T _{deh} [°C]	MSZ [°C]	T _d [°C]
$SrBr_2$	43.8	47.6	3.8	27.6
Sr-LiF	43.8	46.9	3.1	27.6
Sr-ZnF ₂	43.3	45.4	2.1	30.8
Sr-LiCl	43.8	44.2	0.4	31.3
Sr-LiBr	43.7	44.9	1.5	34.8
Sr-CaBr ₂	46.2	48.1	1.9	33.6
Sr-MnBr ₂	45.2	48.1	3.1	29.8
$Sr-ZnBr_2$	44.2	45.9	1.2	34.7
Sr-ZnI ₂	43.8	45.6	1.8	31.8
Sr-K ₂ CO ₃	43.0	47.0	4.0	26.8

During dehydration, temperature and humidity are adjusted simultaneously. This type of cycling will be referred to as high p_d cycling.

The driving force $p_d=p/p_{eq}$ is the relationship between reaction conditions and the thermodynamic equilibrium between the two hydration states. It detrimental for reaction speed and for overcoming potential nucleation barrier present close to equilibrium [25].

3.3. Differential scanning calorimetry

Differential scanning calorimetry (DSC) was conducted using DSC822 by Mettler-Toledo. The device's temperature and heat flow were calibrated using melting point standards (benzophenone, naphthalene, benzoic acid, In and Zn). All measurements were conducted in a dry N_2 atmosphere with a 1.4 L/h flow rate. The DSC thermograms were collected on pristine samples. Powders were grounds and sieved to 50–164 μm fractions and fully hydrated in a desiccator with saturated MgCl $_2$ -6H $_2$ O solution (8 mbar at 21 °C [42]). Approximately 6 mg of the hydrated sample was loaded into a standard 40 μL aluminium pan without a lid. Each measurement started with 15 min of thermal equilibration at -15 °C, followed by a heating step at 1 K/min up to $90\,^{\circ} C$

3.4. Powder X-ray diffraction

The impact of ball milling and cycling on $SrBr_2$ was investigated with powder x-ray diffraction (XRD). This was done in Rigaku Miniflex 600 X-ray diffractometer (Cu K α radiation; Be monochromator, $\lambda=1.5419$ Å, 40 kV, 15 mA) with a D/tex Ultra2 1D detector. The diffractometer is equipped with an Anton-Paar BTS500 heating stage which, together with an in-house built humidifier, controls the atmosphere during the measurement. The measurements were done between 10 and 60 20 with 0.01° step width and $5^{\circ}/min$ scan speed. The data analysis was done in Rigaku PDXL2 software with the aid of Crystallography Open Database (COD).

The ball-milled powders were dried overnight in an oven at 80 $^{\circ}$ C. The dried powders were loaded into a Ni sample holder and once again dried in-situ at 80 $^{\circ}$ C for 30 min to remove the moisture absorbed during powder alignment. The measurement was conducted at 30 $^{\circ}$ C and after 30 min of thermal equilibration. The entire measurement was conducted under constant dry airflow (0 mbar 800 mL/min).

Next, approximately 0.5 g of selected samples were fully hydrated at room temperature in a desiccator with a saturated solution of either MgCl₂·6H₂O (approximately 8 mbar) or LiBr (approximately 1.8 mbar) and subsequently dehydrated in an oven at 80 $^{\circ}$ C. Finally, the dried samples were re-measured according to the procedure described above.

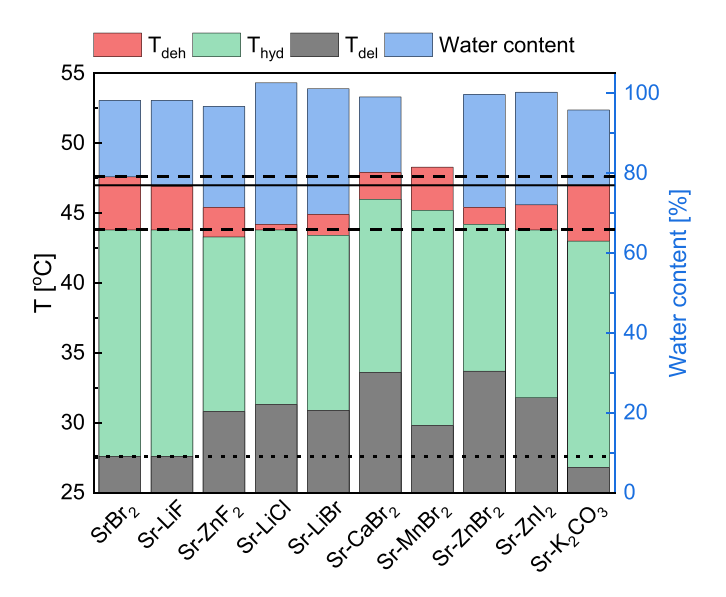


Fig. 2. Summary of data gathered during screening showing hydration (T_{hyd}) and dehydration (T_{deh}) temperatures at 12 mbar at 1 K/min scanning speed, deliquescence temperature (T_d) at 19 mbar and 1 K/min scanning speed and the Measured vs Expected water content during dwell at 30 $^{\circ}\text{C}$ and 12 mbar. The solid horizontal line shows T_{eq} of pure SrBr $_2$ at 12 mbar, and the dashed lines mark the MSZ boundaries established at 12 mbar and 1 K/min. The dotted line indicates T_d of pure SrBr $_2$ at 19 mbar.

3.5. Scanning electron microscopy

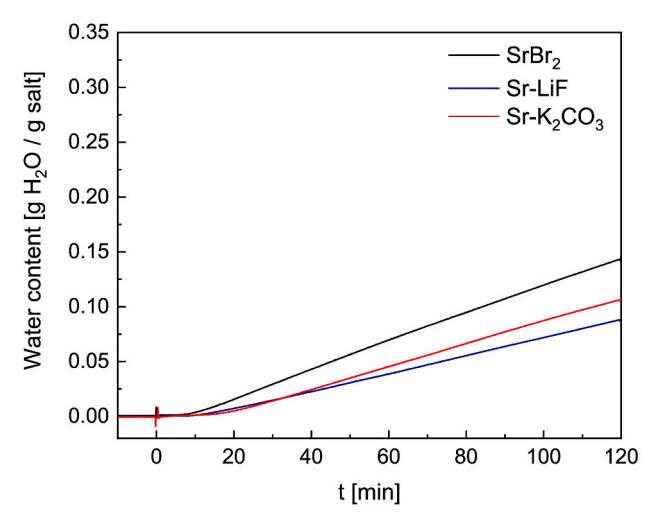
Changes in powder morphology were investigated with scanning electron microscopy (SEM). Before SEM imaging, powder samples were dehydrated in an oven at 80 $^{\circ}\text{C}$. Samples were then fixed to a stub with carbon tape and immediately placed in the SEM to prevent any hydration. The images were taken with JEOL Fei Quanta 600. For the measurement high vacuum, 5 kV accelerating current and 3.0 spot size were used. Both pristine and samples cycled in a TGA were investigated.

4. Results and discussion

4.1. Phase stability

The phase stability of salt mixtures was investigated in two stages by determining the reaction onset points and the deliquescence point. The measured onset temperatures for hydration and dehydration are summarised in Table 4 and Fig. 2. In our evaluation, we consider only the temperature shift greater than 1 K to be significant enough to pursue with further evaluation. It is motivated by the measurement accuracy of ± 0.1 K. Secondly, when judging the water content ratio, we calculate the expected water content based only on the hydration of the salts used during synthesis, while water uptake due to possible deliquescence is not included. Furthermore, deviations within ± 0.02 of the expected value are considered too small to be significant due to measurement error. Therefore, measured water content ± 0.02 above the expected indicates deliquescence of at least one of the salts in the mixture. Finally, although data obtained for Sr-ZnI2 are presented in this section, the salt mixture will not be discussed in the remainder of the paper, as the sample turned yellow after the screening measurement, indicating the decomposition of ZnI_2 .

In the first instance, we compare our measurements with earlier published data. Comparing the measured reaction onset points of pure SrBr₂ with the phase diagram in Fig. 1, shows that present measurements show a wider MSZ compared to the earlier published data [22]. This discrepancy arises from the differences in measurement conditions, where the reaction onset points in the phase diagram have been established at 0.1 K/min versus 1 K/min used in the screening study.



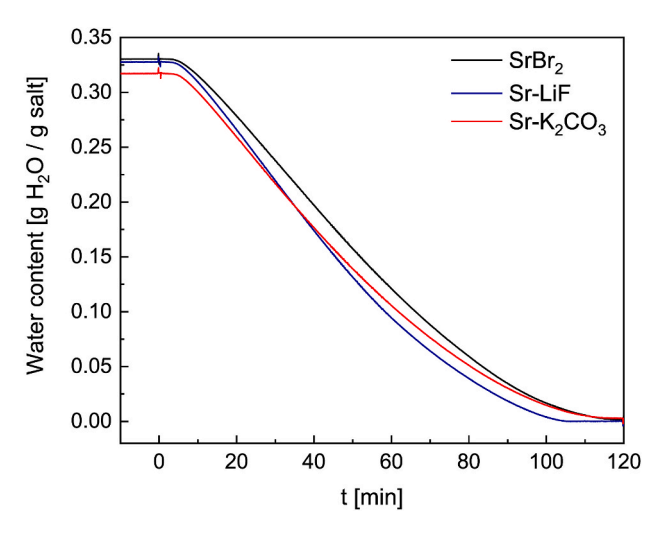


Fig. 3. Isothermal and isobaric a) hydration (45 °C 14 mbar) and b) dehydration (45 °C 9 mbar) kinetics of pure SrBr₂ (black) and salt mixtures (coloured) that have shown no impact on the phase transitions of SrBr₂.

Widening of MSZ with increased scanning speed has been observed in other salt hydrates [44–46]. It indicates that the phase nucleation depends strongly on the time available, which seems to be the case for SrBr₂ 6-1 reaction. Nevertheless, because all measurements have been conducted at identical conditions, results can still be evaluated by comparing salt mixtures to pure SrBr₂.

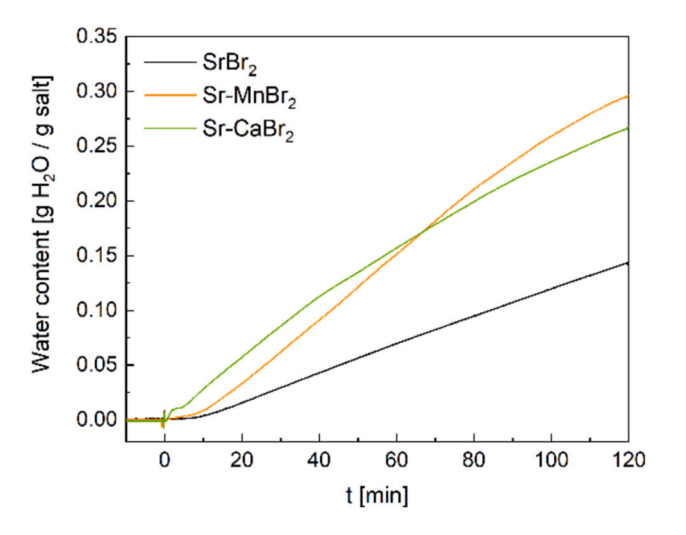
Based on Table 4, we can divide them into 3 categories based on secondary salts that I) Do not impact any of the phase transitions of $SrBr_2$, II) Increase the hydration temperature, and III) Decrease the dehydration temperature.

In category I we find LiF and K_2CO_3 , which did not significantly impact any of the transitions of $SrBr_2$, meaning hydration, dehydration and deliquescence temperatures of $SrBr_2$ are unchanged. LiF has very low solubility, thus a very high deliquescence point and no known hydrates. Hence, it is expected to behave like an inert compound, which is also reflected in the measured water content. Similar results were obtained for the earlier investigated K_2CO_3 -LiF composite [47]. On the other hand, we know that K_2CO_3 is a hygroscopic salt hydrate [25,48], but it is one of the least deliquescent salts investigated. If we look at the onset of deliquescence for $Sr-K_2CO_3$, it is barely affected by the presence of K_2CO_3 . Finally, we cannot exclude the interaction between K_2CO_3 and $SrBr_2$ and the formation of $SrCO_3$ and $SrBr_3$ hoth of which are less deliquescent than $SrBr_2$. The low water uptake supports the theory of side

reactions, as it is less than expected from the hydration of both salts. It means that $Sr-K_2CO_3$ is comparable to Sr-LiF in the sense that we are looking at a mixture of $SrBr_2$ and an inert salt.

In category II we find $CaBr_2$ and $MnBr_2$, which increase the hydration temperature. Interestingly, both salts are the least deliquescent from the bromine-family. Yet they are the only two that significantly and positively impacted the hydration transition. The deliquescence temperature is also increased in both instances, more so for $Sr-CaBr_2$ than the $Sr-MnBr_2$ mixture, which agrees with the MDRH theory. However, the dehydration temperature is also marginally increased.

In category III we have salt mixtures encompassing $Sr-ZnF_2$, Sr-LiCl, Sr-LiBr and $Sr-ZnBr_2$, which have shown a decrease in dehydration onset temperature with respect to pure $SrBr_2$. As we have mentioned before, the measured dehydration onset is partially an artefact of the measurement, since this transition is highly sensitive to the time allowed for phase nucleation. Interestingly, it is most affected by the most hygroscopic salts, LiBr, LiCl and $ZnBr_2$. The samples show a higher water content than expected from hydration only, signifying that the added salt went into deliquescence during the measurement. This was expected given their extreme hygroscopicity. The low DRH of the secondary salt is also reflected in the $T_{\rm del}$ of those salt mixtures, which is also considerably increased. The impact of ZnF_2 is unexpected, based purely on its DRH value. Nevertheless, a previous study has shown that ZnF_2 is prone



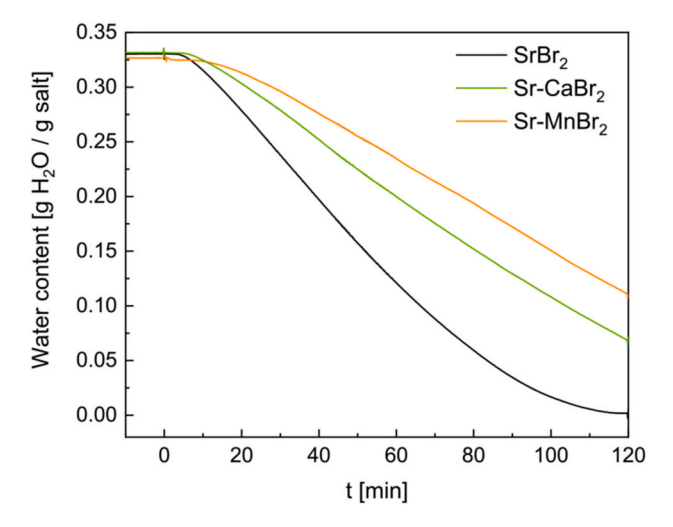
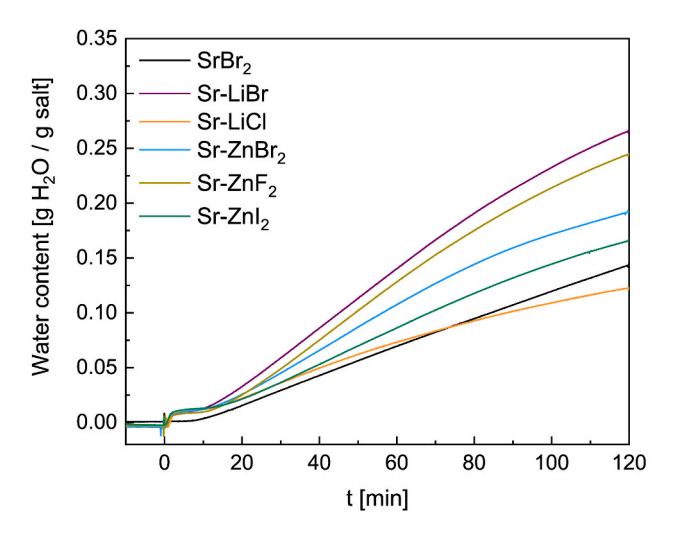


Fig. 4. Isothermal and isobaric a) hydration (45 °C 14 mbar) and b) dehydration (45 °C 9 mbar) kinetics of pure SrBr₂ (black) and salt mixtures (coloured) that have shown increased hydration temperature.



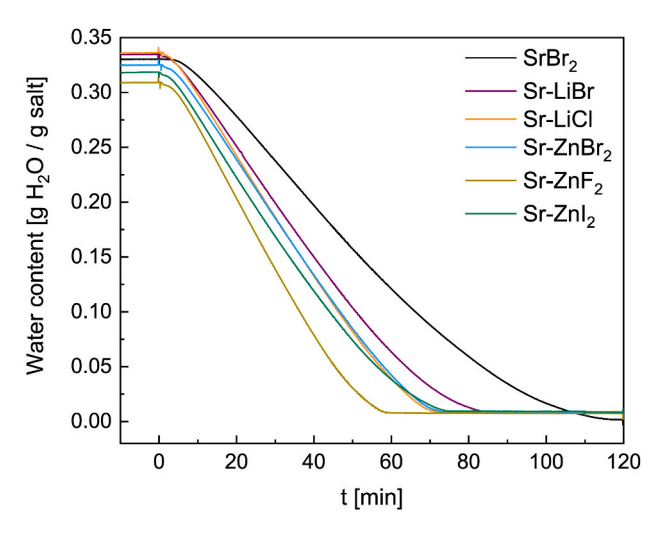


Fig. 5. Isothermal and isobaric a) hydration (45 °C 14 mbar) and b) dehydration (45 °C 9 mbar) kinetics of pure SrBr₂ (black) and salt mixtures (coloured) that have shown decreased dehydration temperature.

to side reactions and hydrolysis in the presence of moisture and other salt hydrates [37]. Given its low water uptake and phase transition behaviour comparable with $Sr-ZnBr_2$, we believe that ZnF_2 has reacted to form $ZnBr_2$, which impacts the phase transition temperatures, and SrF_2 , which lowers the overall absorbed water content as an inert compound.

4.2. Reaction kinetics prior to cycling

In the following evaluation stage, we look at reaction kinetics under isobaric and isothermal conditions (hydration: 45 $^{\circ}$ C and 14 mbar; dehydration: 45 $^{\circ}$ C and 9 mbar). Based on the previous observations, we have divided the salt mixtures into the same 3 categories: I) salts that do not impact phase transitions, I) salts that increase hydration temperature, and III) salts that decrease dehydration temperature.

First, in Fig. 3, we will look at LiF and K₂CO₃ (category I), two salts that did not impact the phase transitions of SrBr₂. If we examine the reaction kinetics, we see that they do not affect them either. Both the hydration and dehydration kinetics of the salt mixtures are very similar to pure SrBr₂. The reaction rates, given by the slopes of the curves, are comparable for both hydration and dehydration. The spread in the plots is due to lower SrBr₂ content in the samples. Due to its high hydration number, any decrease in SrBr₂ mass content will lead to decrease in water content in the sample unless it is compensated by other processes.

In category II (Sr-MnBr2, Sr-CaBr2), we have observed an increased hydration temperature compared to pure SrBr₂. In the first 10 min of hydration kinetics shown Fig. 4, we observe an induction period in pure SrBr₂, which manifests itself by a plateau in mass despite water vapour above equilibrium conditions being present in the system. Both additives shorten this induction period, and the impact of CaBr2 is much more pronounced. There is an immediate mass increase pointing towards the phase transition of CaBr2, and the induction of SrBr2 is reduced by 50%, as the major mass uptake starts in shorter time compared to pure SrBr₂. Based on the screening measurements and the literature [42,49], the transitions we observe in the Sr-CaBr₂ system are most likely a combination of hydration and deliquescence. The shortening of the induction period in the salt mixtures agrees well with the shift in hydration temperature seen in Table 4. It is because the salt mixture starts to hydrate at higher temperatures, the induction period at measurement conditions should be minimal. If we examine the hydration progress in later stages of the measurement, we see that both salt mixtures show more than twice as fast kinetics as pure SrBr2, even though MnBr2 can only hydrate and is not deliquescent under those conditions. The Sr-MnBr2 sample exhibits stable hydration during the

entire measurement (2 h), while the hydration speed of Sr-CaBr₂ drops down after 50 min or approximately 35% conversion.

Looking at dehydration in Fig. 4b, we see that both salt mixtures are 30–50% slower than pure SrBr₂. Under those conditions, MnBr₂ is most likely present as hexahydrate [50]. On the other hand, CaBr₂ should be deliquescent at the start of dehydration, though the dehydration conditions are very close to its DRH value (approximately 15 mbar).

Lastly, we evaluate category III (Sr-LiBr, Sr-ZnBr₂, Sr-LiCl, Sr-ZnF₂) that decrease dehydration temperatures. Although none of the added salts have impacted the hydration temperature, we see that most of them promote faster hydration, as shown in Fig. 5. Interestingly, none of them impacts the induction period, although some of the secondary salts like LiBr and ZnBr₂ undergo deliquescence. The only salt that lowers the hydration rate is LiCl. It could be caused by side reactions and the formation of LiBr and SrCl₂. LiCl has shown to be prone to interaction with the base salt before [47], and although so far LiBr seems to be a promising additive, simultaneous formation of SrCl₂ might counteract it. This salt is known for many hydration states [36] and slow reaction kinetics for some of the transitions [51], which most likely causes the decrease in hydration rate with time observed for Sr-LiCl.

Returning to the remaining candidates, the fastest hydration is observed for Sr-LiBr and Sr-ZnF $_2$, whose behaviour is comparable with Sr-CaBr $_2$ and Sr-MnBr $_2$. Interestingly, the hydration of Sr-ZnBr $_2$ is only 60% faster than SrBr $_2$, although the deliquescence of ZnBr $_2$ is nearly identical with LiBr. This points towards factors other than DRH being important, when aiming for enhanced kinetics.

During dehydration (Fig. 5b) based on the slope we see that all salt mixtures dehydrate 20–60% faster than pure $SrBr_2$, with Sr- ZnF_2 being the fastest and Sr-LiBr the slowest. The difference in the dehydration speed could originate in the differences in the water content in the sample at the start of the dehydration, i.e. more water strongly bound in a crystal structure will take longer to remove. Finally, if we look at the end loading, we see that all salt mixtures retain about 0.01 g of water which could be either water of crystallisation of lower hydrates of the added salt or remnants of a deliquescent phase.

We can exclude several additives from further evaluation, based on results obtained in this part of the screening. Firstly, LiF and K_2CO_3 have no impact on any measured properties. Consequently, they are of no interest for further evaluation. Secondly, LiCl has shown a mixed impact on reaction onset points and kinetics with a strong indication of the formation of several new compounds. Therefore, we have decided not to proceed with the Sr-LiCl salt mixture either. Finally, as mentioned before, Sr-ZnI $_2$ has changed colour from white to yellow during the measurement and also during storage in an airtight container, implying

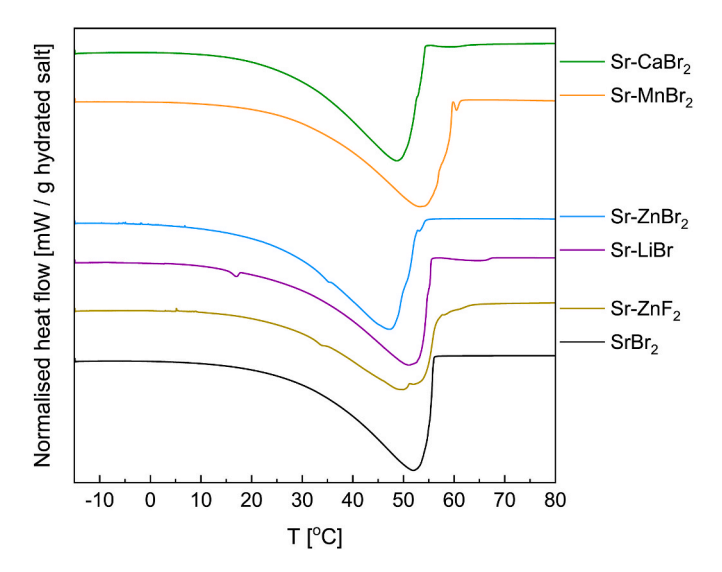


Fig. 6. Heat flow curves measured between -15 – 80 $^{\circ}C$ at 1 K/min in dry N_2 and normalised with respect to hydrated sample weight.

Table 5 Energy density calculated from endothermic peaks in DSC curves between -15 – $80\,^{\circ}\text{C}$.

Sample	Energy density [J/g hydrated sample]	Theoretical energy density [J/g hydrated sample]
SrBr ₂	769	818
Sr-CaBr ₂	772	825
Sr-LiBr	787	816
Sr-MnBr ₂	791	814
Sr-ZnBr ₂	796	810
Sr-ZnF ₂	680	823

accelerated decomposition of ${\rm ZnI_2}$ in the presence of ${\rm SrBr_2}$, so it too will be exempt from further analysis.

In the next stage, we will evaluate salt mixtures with $SrBr_2$ with the other bromide salts and ZnF_2 . The previously described additive selection procedure was based solely on the hygroscopic properties of the additive and the possibility of forming new inert compounds. Consequently, the mixed behaviour we have seen in $SrBr_2$ and bromide salt

mixtures demonstrates that other factors might have to be considered, when choosing a secondary salt hydrate.

4.3. Energy density

In this section, the evaluation of salt mixtures with Br-salts and Sr-ZnF $_2$ continues by measuring the impact of the secondary salt on the energy density of the material. The main interest lies in the impact of deliquescence of the secondary salt on the overall energy density of the sample. It is done by measuring the heat released during sample heating in a DSC. All samples were fully hydrated overnight in a desiccator with saturated MgCl $_2$ -6H $_2$ O solution. The heat flow under a dry N $_2$ atmosphere was registered by scanning from -15 - 80 $^{\circ}$ C at 1 K/min and summarised in Fig. 6. The energy density was calculated from the area of the endothermic peak, assuming a straight baseline, normalised with the hydrated sample mass and listed in Table 5.

The measured energy density of pure $SrBr_2$ agrees with previously measured values [10]. It is about 6% lower than the theoretical energy density of the material. As shown in Table 5, the measured energy densities are comparable with pure $SrBr_2$, and the values expected from the hydration reaction only. This means that the content of the secondary salt is too low to impact the energy density in a measurable manner even if deliquescence of the secondary salt is guaranteed. The only exception is the $Sr-ZnF_2$ sample, whose energy density is about 12% lower than the base salt. It further confirms that ZnF_2 reacts with $SrBr_2$ forming inert compounds.

4.4. Cyclic stability

In the next step, we tested the cyclic stability of the bromide salt mixtures (Sr-LiBr, Sr-ZnBr $_2$, Sr-CaBr $_2$ and Sr-MnBr $_2$). The samples were subjected to 10 (de)hydration cycles at isothermal conditions of 45 °C, with hydration at 19 mbar and dehydration at 0 mbar.

Fig. 7 shows that all bromide salt mixtures can be (de)hydrated at least 10 times without performance loss. Moreover, hydration and dehydration rates increase with cycling by 10–25% between the 1st and 10th cycles. The trends we observe during cycling are comparable with those made in Section 4.2. Both Sr-LiBr and Sr-ZnBr₂ hydrate and dehydrate faster than pure SrBr₂. On the other hand, the effect of CaBr₂ and MnBr₂ is diminished. Therefore, the hydration and dehydration rates of those salt mixtures are comparable with pure SrBr₂, while during screening Sr-CaBr₂ and Sr-MnBr₂ were significantly faster during hydration and significantly slower during dehydration than pure SrBr₂.

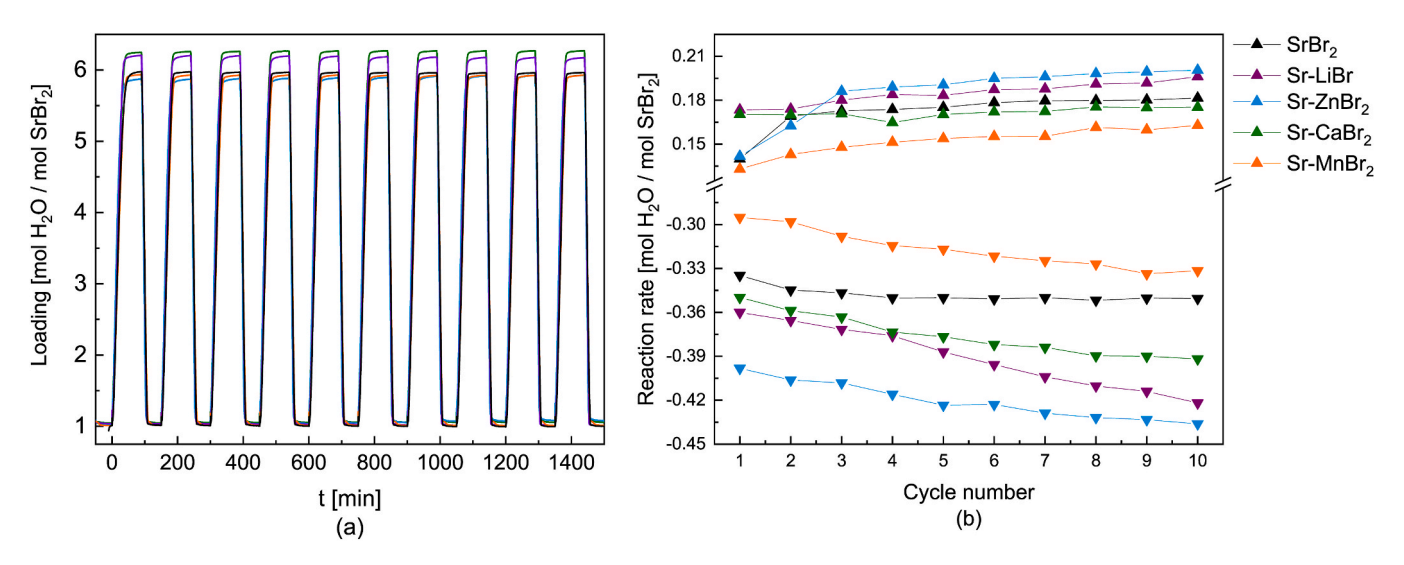


Fig. 7. a) Changes in loading and b) Average (de)hydration rate per cycle between 10 and 90% during cycling measurement at isothermal conditions of 45 °C with hydration at 19 mbar (♠) and dehydration at 0 mbar (▼).

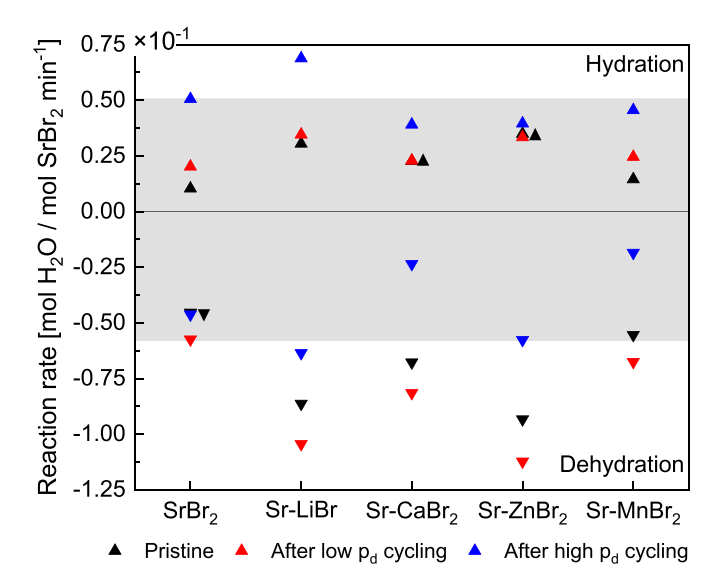


Fig. 8. Reaction rate at 50% conversion measured isobaric and isothermal conditions for hydration (\blacktriangle) at 45 °C and 14 mbar and dehydration (\blacktriangledown) at 45 °C and 9 mbar of pristine samples (black) after high p_d cycling (blue) and after low p_d cycling (red). The grey zone marks reaction rates that do not show significant improvement with respect to pure SrBr₂.

The weakened effect of $CaBr_2$ and $MnBr_2$ is most likely caused by the interplay between the driving force p_d and the DRH of the secondary salt. During the screening, the (de)hydration of $SrBr_2$ was inhibited, i.e. the effect of the secondary salt was much more pronounced. During the cycling measurement, the (de)hydration of $SrBr_2$ was no longer inhibited, so the presence of the secondary salts was no longer vital to overcome the reaction limiting factors such as nucleation battier. Even the two most hygroscopic salts, LiBr and $ZnBr_2$, have limited effect on the phase transitions of $SrBr_2.n$ Moreover, we see that many of the samples have not reached a stable reaction rates within the 10 cycles. For most of the salt mixtures the effect of the secondary salt could become more pronounced with extended cycling, which is needed to thoroughly validate the benefits of a secondary salt. Nevertheless, no signs of degradation are observed in any of the samples.

4.5. Impact of driving force on reaction kinetics

With the cyclic stability proven, we re-evaluated (de)hydration kinetics of the cycled samples at identical conditions as during screening. We will investigate the impact of two cycling conditions, low and high p_d . The cycling conditions discussed in section 4.5 will be referred to as low p_d cycling, since they are conducted relatively close to the equilibrium conditions hence at a low driving force p_d . The second cycling sample conditioning was conducted at a wider temperature range (Hydration at 30 $^{\circ}\text{C}$ and 12 mbar and dehydration at 80 $^{\circ}\text{C}$ and 0 mbar). Those cycling conditions will be referred to as high p_d cycling, as the reaction conditions are further away from the equilibrium. Data gathered during this measurement is presented in the Supplementary Information. The details of reaction conditions are summarised in Table 3 and Fig. 1. The measured reaction rates are summarised in Fig. 8 and compared to reaction rates of pristine samples that did not undergo any cycling.

For pure $SrBr_2$, low p_d cycling has a negligible effect on both hydration and dehydration compared to pristine material. However, in the case of high p_d , cycling we see a significant increase in hydration rate while the dehydration rate remains unchanged. Typically repetitive (de) hydration increases both hydration and dehydration rates [26,48]. It is plausible that different limiting factors govern hydration and dehydration processes, as metastable behaviour has been observed only in the

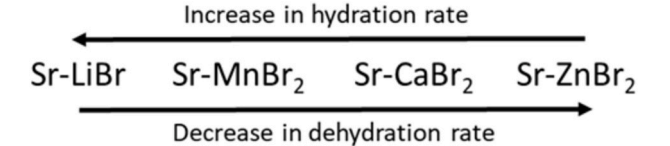


Fig. 9. Impact of high $p_{\rm d}$ cycling on reaction kinetics of ${\rm SrBr_2}$ composities.

case of hydration and not dehydration (see the hatched area in Fig. 1).

If we first look at hydration, we see that low p_d cycling does not affect the reaction rates close to MSZ in a significant way. On the other, after high p_d cycling, the Sr-LiBr sample shows a similar 5-fold improvement as pure $SrBr_2$, while the other samples show no or slight increase in hydration kinetics. Moving onto dehydration, we see that low p_d cycling in many cases doubled the reaction rate compared to pure $SrBr_2$ and all salt mixtures perform better than this salt. On the contrary, the high p_d cycling decreases the dehydration rate for most composites, and the effect is most pronounced for $Sr-CaBr_2$ and $Sr-ZnBr_2$.

Based on those measurements, we can arrange the salts in an order based on an increase in hydration rate and decrease in dehydration rate after high p_d cycling, as shown in Fig. 9.

On top of that, we notice that pure $SrBr_2$ and Sr-LiBr show similar trends in opposition to the other samples. The contrary development of reaction kinetics and its strong dependence on the conditions applied during cycling suggests that other factors than the DRH of the salt hydrates or the number of ions present in the salt mixture need to be considered when selecting the secondary salt. We believe that the large driving force which induces extensive ionic mobility during hydration experienced by samples during high p_d cycling is responsible for the changes presented in Fig. 8.

4.6. Impact of bromide salts on the crystal habit of SrBr₂•H₂O

To better understand the interaction between $SrBr_2$ and the secondary bromide salt, we investigated the pristine and (partially) cycled samples with SEM and PXRD. In both cases, evaluation is conducted after dehydration of the sample to $SrBr_2 \bullet H_2O$.

Fig. 10 presents SEM images of pristine powders (1st column) and cycled samples (2nd and 3rd column) at identical magnification. Pure $SrBr_2$ (1st row) shows hardly any changes with cycling at low $p_d.$ However, the powder cycled at high p_d shows more voids than the pristine sample. We note a very similar development is observed for $Sr-CaBr_2$ and $Sr-MnBr_2$ samples (rows 4 and 5).

On the contrary, salt mixtures with the most deliquescent secondary salts, Sr-LiBr and Sr-ZnBr $_2$ (rows 2 and 3), show a drastically different morphology. Both samples display finer structure than any other powders, characterised by rounded particles a few μm in diameter. In Sr-LiBr, many particles show a laminar structure that partially disappears after cycling at high p_d . Similar formations are present in Sr-ZnBr $_2$ but to a much smaller extent.

In the next stage, we look deeper into the crystal habit by employing XRD. All pristine samples in Fig. 11a present similar diffraction patterns, and only SrBr₂ \bullet H₂O (COD 1528458 [52]) is detected. Pure SrBr₂, Sr-CaBr₂ and Sr-ZnBr₂ have patterns that are most like the published pattern, with the characteristic three peaks decreasing in intensity between 28.5 and 31.9 20.

After single hydration at low p_d (Fig. 11b), all patterns show negligible changes. However, after single hydration at high p_d (Fig. 11c), the pure $SrBr_2$ and $Sr-MnBr_2$ patterns show only minor changes compared to pristine samples, while the other patterns show a significant transformation. All three samples (Sr-LiBr, $Se-ZnBr_2$ and $Sr-CaBr_2$) show preferential orientation towards (2,0,0) orientation, characterised by peaks at 15.5 and 31.2 20 (marked with a black arrow in Fig. 11c). It shows that highly deliquescent bromide salts can affect the structure of $SrBr_2$. Moreover, adding $ZnBr_2$ and LiBr leads to peak splitting,

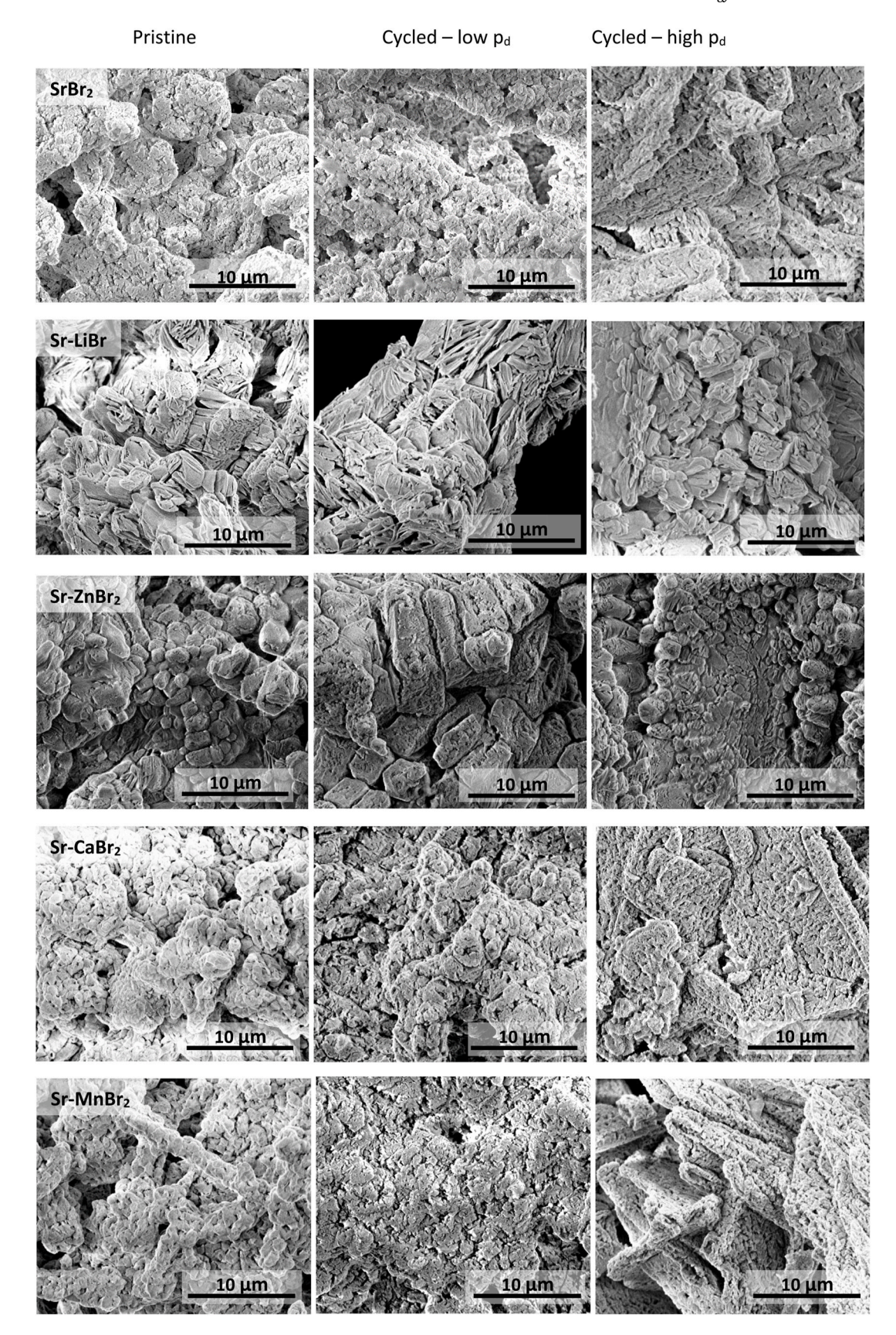


Fig. 10. SEM images at $5000 \times$ magnification of pristine (left), cycled at 45 °C (middle) and cycled between 30 and 80 °C (right) powders of pure SrBr₂, Sr-LiBr, Sr-ZnBr₂, Sr-CaBr₂ and Sr-MnBr₂.

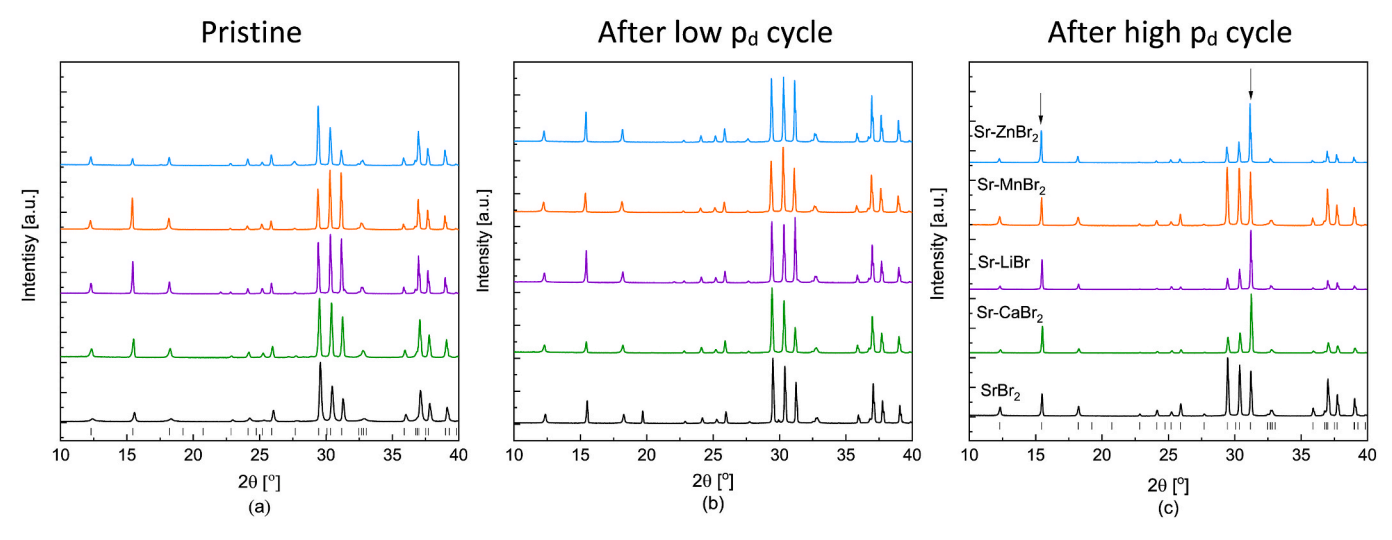


Fig. 11. XRD patterns of $SrBr_2 H_2O$ salt mixtures a) right after synthesis and b) after 1 (de) hydration cycle at low p_d c) after 1 (de)hydration cycle at high p_d . Black arrows show (2,0,0) planes, which exhibit the greatest change.

indicating symmetry changes that could be related to the new structures observed in SEM images.

Although the formation of new salts is impossible in the bromide salt mixtures, which is confirmed by the lack of new reflections in the XRD spectra, a cation exchange between two salts could occur. At high p_d , the

presence of large amounts of water vapour in the system will induce high ionic mobility. All the divalent cations in the secondary salts $(Zn^{2+}, Ca^{2+}, Mn^{2+})$ have ionic radii [53] that satisfy the Goldschmidt for ion substitution. The only system, where such interaction is impossible is Sr-LiBr, as Li-ion is monovalent. It is also the only system that presents

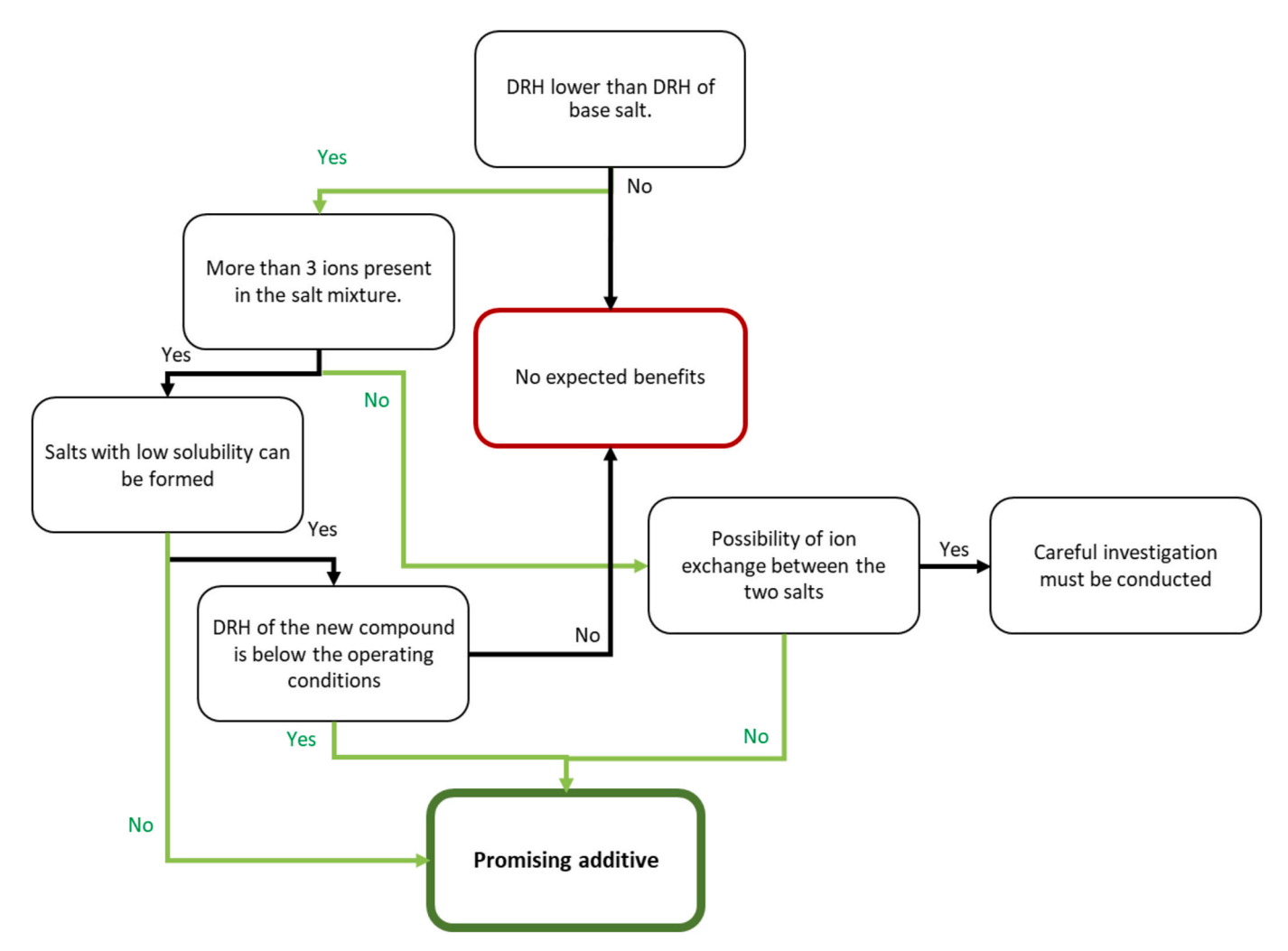


Fig. 12. Flow chart visualising the secondary salt selection process adapted from [37].

an enhanced behaviour under all investigated conditions. We therefore believe that the increase or decrease in reaction kinetics induced by reaction conditions (see Fig. 8) are due to cation exchange between Sr^{2+} and the corresponding divalent cation of the secondary salt. This exchange is most likely the reason why CaBr_2 and ZnBr_2 have a limited effect on the kinetics of SrBr_2 after high p_d cycling.

5. Conclusion

In this work, we have investigated the impact of hygroscopic salt hydrates on the $SrBr_2$ 1-6 (de)hydration reaction considered for TCHS. To select the hygroscopic salt, we used an approach previously developed on $K_2CO_3.$ We tested 9 different salt mixtures and found that the previously described approach can also be used on other base salts. The points that can be directly carried through from the previously developed method are:

- Non-deliquescent salts do not contribute to the phase transition of the base salt in any way, thus they should not be used.
- Deliquescent salts that can react with the base salt and form new insoluble salts lower the energy density and should not be used.
- Salts that share a common ion with the base salt have the highest chance of success.

Nevertheless, additional points of attention should be added to the selection procedure. Namely, in addition to evaluating the likelihood of salt interaction and formation of new salts, the possibility of ion substitution should be considered. This mode of interaction might not be directly adverse to phase transitions of the salt mixtures. As we have seen it can lead to limited modification of the wetting layer and limited impact on kinetics, as in the case of Sr-ZnBr $_2$. On the other hand, the effect can be much more severe than that as in the case of dehydration of Sr-CaBr $_2$ and Sr-MnBr $_2$. Those interactions have been seen only when the salts have been exposed to high p_d conditions. This underlines the importance of water and ionic mobility in the system as it not only facilitates the phase transitions in the base salt but also the degree of interaction between the base and secondary salt.

The second point that needs to be examined considers salt hydrates with many hydration states. Using those compounds as a secondary salt can be much more challenging than salts with a single hydration transition, as we have seen in the case of CaBr₂ and MnBr₂. Reaction hysteresis present in the individual phase transitions of the secondary salt might affect the base salt, lead to water retention if insufficient heat is supplied during dehydration or delay desired deliquescence if formation of the highest hydrate of the secondary hydrate is inherently slow. The many additionally phase transitions might present competition for water the base salt, all of which adds an extra level of complexity of the system.

The secondary salt selection procedure can be summarised in a form of a flow chart presented in Fig. 12. Nevertheless, this procedure should be taken only as a general guideline when applying to other salts as other interactions between salts could exist that are not included in this diagram.

Overall, using small amounts of highly hygroscopic salts is a promising approach to augment the phase transition behaviour of salt hydrates considered for TCHS. This approach enables modification of reaction onset points and enhancement of kinetics without sacrificing energy density. It also opens up possibilities for other salt hydrates that are much more challenging to work with under conditions dictated by the domestic environment.

CRediT authorship contribution statement

Natalia Mazur: Writing – review & editing, Writing – original draft, Visualization, Validation, Supervision, Methodology, Investigation, Formal analysis, Data curation, Conceptualization. **Isidoros Kotinis:** Validation, Methodology, Investigation. **Henk Huinink:** Writing –

review & editing, Supervision, Project administration, Funding acquisition, Conceptualization. **Hartmut Fischer:** Writing – review & editing, Conceptualization. **Olaf Adan:** Writing – review & editing, Supervision, Funding acquisition, Conceptualization.

Declaration of competing interest

The authors declare that they have no known competing financial interests or personal relationships that could have appeared to influence the work reported in this paper.

Data availability

Data will be made available on request.

Acknowledgements

This publication is part of the project Mat4Heat with project number 739.017.014 of the research programme Mat4Sus which is financed by the Netherlands Research Council (NWO).

The authors thank Hans Dalderop and dr. Pim Donkers for their support.

Appendix A. Supplementary data

Supplementary data to this article can be found online at $\frac{\text{https:}}{\text{doi.}}$ org/10.1016/j.solmat.2024.112748.

References

- [1] IEA." https://www.iea.org/regions/europe (accessed March. 23, 2022)...
- [2] REmap Energy Demand and Supply by Sector." https://www.irena.org/Statistic s/View-Data-by-Topic/Energy-Transition/REmap-Energy-Demand-and-Supply-by-Sector (accessed March. 23, 2022).
- [3] Energy consumption in households." https://ec.europa.eu/eurostat/statistics-e xplained/index.php?title=Energy_consumption_in_households (accessed March 23, 2022).
- [4] L. Scapino, H.A. Zondag, J. Van Bael, J. Diriken, C.C.M. Rindt, Sorption heat storage for long-term low-temperature applications: a review on the advancements at material and prototype scale, Appl. Energy 190 (2017) 920–948, https://doi. org/10.1016/j.apenergy.2016.12.148.
- [5] W. Li, J.J. Klemeš, Q. Wang, M. Zeng, Salt hydrate–based gas-solid thermochemical energy storage: current progress, challenges, and perspectives, Renew. Sustain. Energy Rev. 154 (Feb. 2022) 111846, https://doi.org/10.1016/j. rser.2021.111846.
- [6] T.X. Li, R.Z. Wang, T. Yan, T.F. Ishugah, Integrated energy storage and energy upgrade, combined cooling and heating supply, and waste heat recovery with solid-gas thermochemical sorption heat transformer, Int. J. Heat Mass Tran. 76 (Sep. 2014) 237–246, https://doi.org/10.1016/J. LJHEATMASSTRANSFER.2014.04.046.
- [7] T. Li, R. Wang, J. K. Kiplagat, and Y. T. Kang, "Performance analysis of an integrated energy storage and energy upgrade thermochemical solid–gas sorption system for seasonal storage of solar thermal energy," Energy, vol. 50, no. 1, pp. 454–467, Feb. 2013, doi: 10.1016/J.ENERGY.2012.11.043..
- [8] B. Michel, N. Mazet, S. Mauran, D. Stitou, J. Xu, Thermochemical process for seasonal storage of solar energy: characterization and modeling of a high density reactive bed, Energy 47 (1) (2012) 553–563, https://doi.org/10.1016/j. energy.2012.09.029.
- [9] K.E. N'Tsoukpoe, T. Schmidt, H.U. Rammelberg, B.A. Watts, W.K.L. Ruck, A systematic multi-step screening of numerous salt hydrates for low temperature thermochemical energy storage, Appl. Energy 124 (2014) 1–16, https://doi.org/ 10.1016/j.apenergy.2014.02.053.
- [10] A. Fopah-Lele, J.G. Tamba, A review on the use of SrBr2-6H2O as a potential material for low temperature energy storage systems and building applications, Sol. Energy Mater. Sol. Cells 164 (2017) 175–187, https://doi.org/10.1016/j. solmat.2017.02.018. February.
- [11] B. Michel, P. Neveu, N. Mazet, Comparison of closed and open thermochemical processes, for long-term thermal energy storage applications, Energy 72 (Aug. 2014) 702–716, https://doi.org/10.1016/J.ENERGY.2014.05.097.
- [12] Y.N. Zhang, R.Z. Wang, Y.J. Zhao, T.X. Li, S.B. Riffat, N.M. Wajid, Development and thermochemical characterizations of vermiculite/SrBr2 composite sorbents for low-temperature heat storage, Energy 115 (Nov. 2016) 120–128, https://doi.org/ 10.1016/J.ENERGY.2016.08.108.
- [13] B. Ding, C. Xu, Z. Liao, F. Ye, Study on long-term thermochemical thermal storage performance based on SrBr2-expanded vermiculite composite materials, J. Energy Storage 42 (Oct. 2021) 103081, https://doi.org/10.1016/J.EST.2021.103081.

- [14] E. Courbon, et al., A new composite sorbent based on SrBr2 and silica gel for solar energy storage application with high energy storage density and stability, Appl. Energy 190 (Mar. 2017) 1184–1194, https://doi.org/10.1016/J. APENERGY.2017.01.041.
- [15] P. D'Ans, et al., A new strontium bromide MOF composite with improved performance for solar energy storage application, J. Energy Storage 25 (Oct. 2019) 100881, https://doi.org/10.1016/J.EST.2019.100881.
- [16] L. Calabrese, V. Brancato, V. Palomba, A. Frazzica, L.F. Cabeza, Innovative composite sorbent for thermal energy storage based on a SrBr2-6H2O filled silicone composite foam, J. Energy Storage 26 (2019) 100954, https://doi.org/10.1016/j. est.2019.100954. July.
- [17] S. Mauran, H. Lahmidi, V. Goetz, Solar heating and cooling by a thermochemical process. First experiments of a prototype storing 60 kW h by a solid/gas reaction, Sol. Energy 82 (7) (Jul. 2008) 623–636, https://doi.org/10.1016/J. SOLENER 2008.01.002.
- [18] H. Lahmidi, S. Mauran, V. Goetz, Definition, test and simulation of a thermochemical storage process adapted to solar thermal systems, Sol. Energy 80 (7) (2006) 883–893, https://doi.org/10.1016/j.solener.2005.01.014.
- 19] Y.J. Zhao, R.Z. Wang, Y.N. Zhang, N. Yu, Development of SrBr2 composite sorbents for a sorption thermal energy storage system to store low-temperature heat, Energy 115 (2016) 129–139, https://doi.org/10.1016/j.energy.2016.09.013.
- [20] S. Salviati, F. Carosio, G. Saracco, A. Fina, Hydrated salt/graphite/polyelectrolyte organic-inorganic hybrids for efficient thermochemical storage, Nanomaterials 9 (3) (2019) 15121, https://doi.org/10.3390/nano9030420.
- [21] S. Salviati, et al., Ice-templated nanocellulose porous structure enhances thermochemical storage kinetics in hydrated salt/graphite composites, Renew. Energy 160 (2020) 698–706, https://doi.org/10.1016/j.renene.2020.07.036.
- [22] N. Mazur, et al., Impact of polymeric stabilisers on the reaction kinetics of SrBr2, Sol. Energy Mater. Sol. Cells 238 (May 2022) 111648, https://doi.org/10.1016/j. solmat.2022.111648.
- [23] T. Esaki, N. Kobayashi, Reaction rate characteristics of SrBr₂ hydration system for Chemical heat Pump cooling mode, J. Mater. Sci. Chem. Eng. 4 (2) (2016) 106–115, https://doi.org/10.4236/msce.2016.42012.
- [24] M. Richter, E.M. Habermann, E. Siebecke, M. Linder, A systematic screening of salt hydrates as materials for a thermochemical heat transformer, Thermochim. Acta 659 (2018) 136–150. https://doi.org/10.1016/j.tca.2017.06.011. February 2017.
- [25] L.C. Sögütoglu, et al., Understanding the hydration process of salts: the impact of a nucleation barrier, Cryst. Growth Des. 19 (4) (2019) 2279–2288, https://doi.org/ 10.1021/acs.ced.8b01908.
- [26] C.J. Ferchaud, Experimental Study of Salt Hydrates for Thermochemical Seasonal Heat Storage, Eindhoven University of Technology, Eindhoven, 2016.
- [27] N. Mazur, H. Huinink, H. Fischer, P. Donkers, O. Adan, Accelerating the reaction kinetics of K2CO3 through the addition of CsF in the view of thermochemical heat storage, Sol. Energy 242 (Aug. 2022) 256–266, https://doi.org/10.1016/j. solener.2022.07.023.
- [28] J. Houben, Accelerating Thermochemical Energy Storage by Doping, Eindhoven University of Technology, 2023.
- [29] K. Posern, C. Kaps, Calorimetric studies of thermochemical heat storage materials based on mixtures of MgSO4 and MgCl2, Thermochim. Acta 502 (1–2) (2010) 73–76, https://doi.org/10.1016/j.tca.2010.02.009.
- [30] K. Korhammer, et al., Sorption and thermal characterization of composite materials based on chlorides for thermal energy storage, Appl. Energy 162 (2016) 1462 1472 https://doi.org/10.1016/j.npngergy.2015.08.037
- 1462–1472, https://doi.org/10.1016/j.apenergy.2015.08.037.
 [31] H. Jarimi, et al., Materials characterization of innovative composite materials for solar-driven thermochemical heat storage (THS) suitable for building application, Int. J. Low Carbon Technol. 13 (1) (Sep. 2018) 30–42, https://doi.org/10.1093/iilet/cty017
- [32] A. Ur Rehman, M. Khan, Z. Maosheng, Hydration behavior of MgSO 4 -ZnSO 4 composites for long-term thermochemical heat storage application Hydration behavior of MgSO 4 ZnSO 4 composites for long-term thermochemical heat storage application, J. Energy Storage 26 (October) (2019) 101026, https://doi.org/10.1016/j.est.2019.101026.
- [33] K. Posern, C. Kaps, Influences of salt hydrate mixtures and pore sizes on the sorption heat of composite TES materials, in: Proc. 11th Int. Conf. Therm. Energy Storage (Effstock 2009), 2009, pp. 1–6, l.

- [34] W. Li, M. Zeng, Q. Wang, Development and performance investigation of MgSO4/ SrCl2 composite salt hydrate for mid-low temperature thermochemical heat storage, Sol. Energy Mater. Sol. Cells 210 (Jun. 2020) 110509, https://doi.org/ 10.1016/j.solmat.2020.110509. March.
- [35] H.U. Rammelberg, M. Myrau, T. Schmidt, W.K. Ruck, An Optimization of Salt Hydrates for Thermochemical Heat Storage," Touka Shobo Innov. Mater. Process. Energy Syst. Bidyut Baran Saha, Michihisa Koyama, Yasuyuki Tak. Yoshinori Hamamoto, Tak. Miyazaki, Kohno Masamichi, Kohei Ito, IMPRES, 2013, p. 550. _555
- [36] J. Houben, A. Shkatulov, H. Huinink, H. Fischer, O. Adan, Caesium doping accelerates the hydration rate of potassium carbonate in thermal energy storage, Sol. Energy Mater. Sol. Cells 251 (Mar. 2023) 112116, https://doi.org/10.1016/j. solmat.2022.112116.
- [37] N. Mazur, H. Huinink, H. Fischer, and O. Adan, "Under Review: A Systematic Deliquescent Additive Selection Approach for Enhancement of Reaction Kinetics of Thermochemical Heat Storage Materials. - Under review.".
- [38] T. Yan, et al., Ultrahigh-energy-density sorption thermal battery enabled by Graphene Aerogel-based composite sorbents for thermal energy Harvesting from Air, ACS Energy Lett. 6 (5) (May 2021) 1795–1802, https://doi.org/10.1021/ ACSENERGYLETT.1C00284/ASSET/IMAGES/LARGE/NZ1C00284_0003. JPEG.
- [39] M.-M. Druske, The Reactions of Mixed Salts in Advanced Heat Storage Systems, Technische Universität München, Ludiwg-Maximilians-Universität München, 2018
- [40] G.A. Lane, Phase change materials for energy storage nucleation to prevent supercooling, Sol. Energy Mater. Sol. Cells 27 (2) (1992) 135–160, https://doi.org/ 10.1016/0927-0248(92)90116-7.
- [41] Bissell, Strontium Bromide Phase Change Material, 1992.
- [42] L. Greenspan, Humidity fixed points of binary saturated Aqueous solutions, J. Res. Natl. Bur. Stand. - A. Phys ics Chem. 82A (1) (1976) 89–96.
- [43] G.M. Richardson, R.S. Malthus, Salts for static control of humidity at relatively low levels, J. Appl. Chem. 5 (10) (1955) 557–567, https://doi.org/10.1002/ jctb.5010051006.
- [44] J. Xu, T. Li, T. Yan, J. Chao, R. Wang, Dehydration kinetics and thermodynamics of magnesium chloride hexahydrate for thermal energy storage, Sol. Energy Mater. Sol. Cells 219 (March 2020) 2021.
- [45] T.S. Yan, T.X. Li, J.X. Xu, J.W. Chao, Understanding the transition process of phase change and dehydration reaction of salt hydrate for thermal energy storage, Appl. Therm. Eng. 166 (March 2019) 2020, https://doi.org/10.1016/j. applthermaleng.2019.114655.
- [46] T. Liavitskaya, S. Vyazovkin, Delving into the Kinetics of Reversible Thermal Decomposition of Solids Measured on Heating and Cooling, 2017, https://doi.org/ 10.1021/acs.jpcc.7b05066.
- [47] N. Mazur, Boosting Power of Salt Hydrates for Heat Storage, 2023.
- [48] L.C. Sögütoglu, P.A.J. Donkers, H.R. Fischer, H.P. Huinink, O.C.G. Adan, In-depth investigation of thermochemical performance in a heat battery: cyclic analysis of K2CO3, MgCl2and Na2S, Appl. Energy 215 (2018) 159–173, https://doi.org/ 10.1016/j.apenergy.2018.01.083.
- [49] L. Glasser, Thermodynamics of inorganic hydration and of humidity control, with an extensive database of salt hydrate pairs, J. Chem. Eng. Data 59 (2) (2014) 526–530, https://doi.org/10.1021/je401077x.
- [50] P.A.J. Donkers, L.C. Sögütoglu, H.P. Huinink, H.R. Fischer, O.C.G. Adan, A review of salt hydrates for seasonal heat storage in domestic applications, Appl. Energy 199 (2017) 45–68, https://doi.org/10.1016/j.apenergy.2017.04.080.
 [51] M.A.R. Blijlevens, et al., A study of the hydration and dehydration transitions of
- SrCl2 hydrates for use in heat storage, Sol. Energy Mater. Sol. Cells 242 (Aug. 2022) 111770, https://doi.org/10.1016/j.solmat.2022.111770.
- [52] M. Dyke and R. L. Sass, "The Crystal Structure of Strontium Bromide Monohydrate," Accessed: May 11, 2022. [Online]. Available: https://pubs.acs.org/sharingguidelines..
- [53] R.D. Shannon, Revised effective ionic radii and systematic studies of interatomic distances in halides and chalcogenides, Acta Crystallogr. Sect. A Cryst. physics, diffraction, Theor. Gen. Crystallogr. 32 (5) (1976) 751–767.